

---

# Diffusion<sup>2</sup>: Dynamic 3D Content Generation via Score Composition of Orthogonal Diffusion Models

---

Zeyu Yang\* Zijie Pan\* Chun Gu Li Zhang<sup>†</sup>

Fudan University

<https://github.com/fudan-zvg/diffusion-square>

## Abstract

Recent advancements in 3D generation are predominantly propelled by improvements in 3D-aware image diffusion models which are pretrained on Internet-scale image data and fine-tuned on massive 3D data, offering the capability of producing highly consistent multi-view images. However, due to the scarcity of synchronized multi-view video data, it is impractical to adapt this paradigm to 4D generation directly. Despite that, the available video and 3D data are adequate for training video and multi-view diffusion models separately that can provide satisfactory dynamic and geometric priors respectively. To take advantage of both, this paper present *Diffusion<sup>2</sup>*, a novel framework for dynamic 3D content creation that reconciles the knowledge about geometric consistency and temporal smoothness from these models to directly sample dense multi-view multi-frame images which can be employed to optimize continuous 4D representation. Specifically, we design a simple yet effective denoising strategy via score composition of pretrained video and multi-view diffusion models based on the probability structure of the target image array. Owing to the high parallelism of the proposed image generation process and the efficiency of the modern 4D reconstruction pipeline, our framework can generate 4D content within few minutes. Additionally, our method circumvents the reliance on 4D data, thereby having the potential to benefit from the scaling of the foundation video and multi-view diffusion models. Extensive experiments demonstrate the efficacy of our proposed framework and its ability to flexibly handle various types of prompts.

## 1 Introduction

Spurred by the advances from generative image models [14, 36, 37, 18, 55], automatic 3D content creation [29, 44, 39, 15] has witnessed remarkable progress in terms of efficiency, fidelity, diversity, and controllability. Coupled with the breakthroughs in 4D representation [51, 47, 9], these advances further foster substantial development in dynamic 3D content generation [35, 1, 16, 57, 31, 11], which holds significant value across a wide range of applications in animation, film, game, and MetaVerse.

Recently, 3D content generation has achieved considerable breakthroughs in efficiency. Some works [22, 23, 34, 43, 40] inject stereo knowledge into the image generation model, enabling these 3D-aware image generators to produce consistent multi-view images, thereby effectively stabilizing and accelerating the optimization. Other efforts [15, 7, 42, 58, 38] attempt to directly generate 3D representations, such as triplane [6] or Gaussian splatting [19]. However, the efficiency improvement from these works is largely data-driven [49, 30, 54, 8]. Consequently, it is infeasible to adapt them to

---

\*Equally contributed

<sup>†</sup>Li Zhang (lizhangfd@fudan.edu.cn) is the corresponding author with School of Data Science, Fudan University.

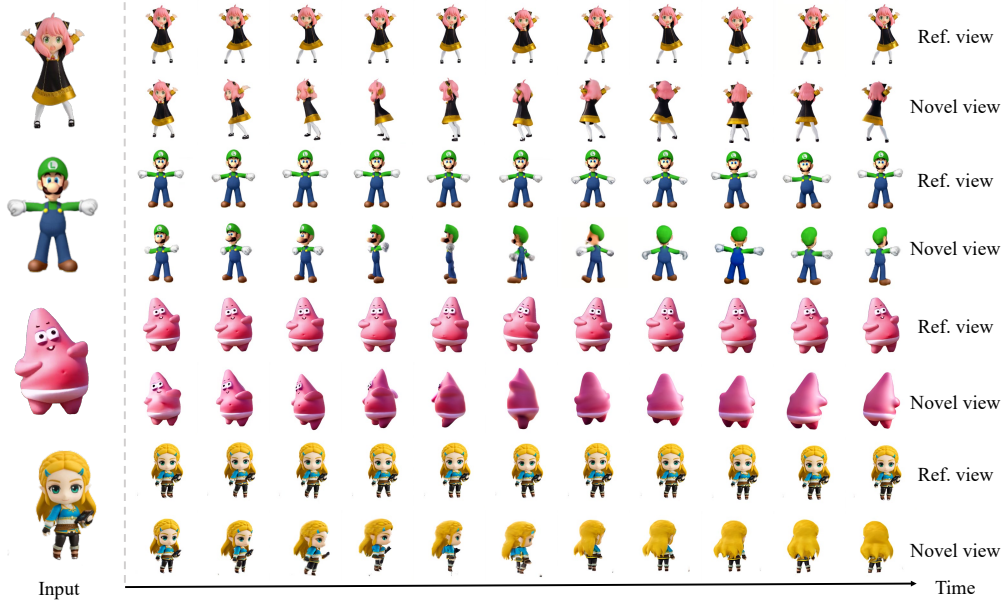


Figure 1: *Diffusion*<sup>2</sup> is designed to generate dynamic content by creating a dense multi-frame multi-view image matrix in a highly parallel denoising diffusion process with the combination of the foundation video diffusion model and multi-view diffusion model. The generated image can be used to construct a full 4D representation by feeding them into an off-the-shelf 4D reconstruction pipeline.

4D generation due to the scarcity of synchronized multi-view video data. Therefore, most existing 4D generation works [16, 53, 31] still adopt the score distillation sampling (SDS) approach and suffer from slow or unstable optimization.

However, despite the paucity of 4D data, there are vast available monocular video data and static multi-view image data. Existing works have demonstrated that it is feasible to train diffusion-based generative models learning the distribution of these two classes of data independently [42, 23, 40, 4, 3]. Considering that video diffusion model stores the prior of motion and temporal smoothness, and multi-view diffusion model has sound knowledge of geometrical consistency, combining the two generative models to generate 4D assets becomes a highly promising and appealing approach.

To leverage both of them, inspired by the previous work [2, 21], we propose a novel 4D generation framework that reconciles the video and multi-view diffusion priors to directly sample multi-frame multi-view image arrays imitating the photographing process of 4D object. To demonstrate how we realize this combination, we assume that such an image matrix  $\mathcal{I}$  has a nice structure: the elements  $\mathcal{I}_{i,j}$  and  $\mathcal{I}_{k,l}$  not in the same row and column ( $i \neq k, j \neq l$ ) are conditionally independent of each other given  $\mathcal{I}_{i,l}$  or  $\mathcal{I}_{k,j}$ . Based on this property, we design a simple yet effective denoising sampling strategy in which the estimated score is just the convex combination of the scores predicted by two foundation diffusion models. Our formulation is easy to adapt to various prompts including reference image, single-view video, and static 3D content. Unlike the existing SDS-based counterparts, *Diffusion*<sup>2</sup> is highly parallel. Combined with the efficient 4D reconstruction pipeline, our method can generate high-fidelity and diverse 4D assets within just a few minutes. Besides, our approach can also potentially benefit from the further advancement of foundation diffusion models [5].

Our contributions are threefold: **(i)** We present a novel 4D content generation approach that achieves zero-shot generation of realistic multi-view multi-frame image arrays, which can be integrated with an off-the-shelf modern 4D reconstruction pipeline to efficiently create 4D content. **(ii)** We identify the conditional independence within elements constituting the image arrays. Based on it, we devise a simple yet effective joint denoising strategy that combines video diffusion model and multi-view diffusion model to directly sample multi-view multi-frame images from their natural joint distribution. **(iii)** Systematic experiments demonstrate that our proposed method can achieve satisfactory results under different types of prompts, including single image, single-view video, and static 3D content.

## 2 Related work

**3D generation** 3D generation aims at creating static 3D content from different type of conditions like text or reference image. Early efforts employed GAN-based approaches [10, 33]. Recently, significant breakthroughs have been achieved with diffusion models [14]. DreamFusion [29] introduced score distillation sampling (SDS) to unleash the creativity in diffusion models. A series of subsequent works [44, 34, 43, 27, 39, 52] continuously address challenges such as multi-face Janus issues and slow optimization. On the other hand, with the development of large scale 3D datasets [54, 8], many works try to directly generate 3D contents by using diffusion models. Some studies [26, 17, 15, 38, 45] have explored the direct generation of 3D representations. Another line of research [22, 23, 24, 7, 40] focuses on generating multi-view images with sufficient 3D consistency to be used for reconstruction. We also adopt this approach of directly generating consistent images for reconstruction. But unlike the above 3D counterparts, there is no large-scale multi-view synchronized video data. Therefore, we opt to combine geometrical consistency priors and video dynamic priors to generate images.

**Video generation** Video generation is an active field that has gained increasing popularity. Recent diffusion-based methods have exhibited unprecedented levels of realism, diversity, and controllability. Video LDM [4] is the pioneer work to apply the latent diffusion framework [32] to video generation. The subsequent work SVD [3] followed its architecture and made effective improvements to the training recipe. W.A.L.T [12] employed a transformer with window attention tailored for spatiotemporal generative modeling to generate high-resolution videos. VDT [25] introduced the video diffusion transformer and a spatial-temporal mask mechanism to flexibly capture long-distance spatiotemporal context. The recently introduced SORA [5] demonstrated a remarkable capability to generate long videos with intuitively physical fidelity. Models trained on large-scale video data can generate videos with realistic dynamics. Besides, video diffusion models can also provide effective prior for 3D generators [7, 13, 42]. Therefore, we build our method on this flourishing domain.

**4D generation** Animating category-agnostic objects is challenging and has drawn considerable attention from both academia and industry. Unlike 3D generation, 4D generation requires both consistent geometry and realistic dynamics. Recent works on this domain can be categorized based on the input condition. Some of them create 4D content from text or single image. For instance, MAV3D [35] first employs SDS in text-to-4D tasks. 4D-fy [1] hybridizes different diffusion priors during SDS training. But they suffer from extremely slow generation. DreamGaussian4D [31] adopts deformable 3D Gaussian [51] as the underlying 4D representation and exports mesh for texture refinement, significantly improving efficiency. Another line of work predicts dynamic objects from a single-view video with largely dictated motion. Consistent4D [16] proposes to use SDS approach for geometry consistency and frame interpolation loss for temporal continuity. 4DGen [53] further grounds the 4D content creation with pseudo labels. Efficient4D [28] mimics a photogrammetry-based neural volumetric video reconstruction pipeline by directly generating multi-view videos for reconstruction. Although we share the same SDS-free design, Efficient4D possesses a strong architectural preference for the fundamental diffusion model and is incapable of synthesizing novel dynamics. Compared to previous works, our framework can efficiently generate diverse 4D contents from different input prompts, avoiding the slow and unstable optimization. In addition, our method has the potential to continuously benefit from the scalability of underlying diffusion models.

## 3 Method

As depicted in Figure 2, the proposed 4D generation framework *Diffusion*<sup>2</sup> adopts a two-stage pipeline: dense observation synthesis followed by reconstruction. In Section 3.1 (stage-1), we will elaborate on how to generate dense multi-view multi-frame images for reconstruction through a highly parallelizable denoising process by reconciling the pretrained video diffusion prior and multi-view diffusion prior, and why it is feasible. In Section 3.2 (stage-2), we will briefly introduce how to robustly reconstruct 4D content from the images produced in the first stage.

### 3.1 Image matrix generation

In this stage, our goal is to generate dense multi-frame multi-view images for reconstruction, which can be denoted as a matrix of images:

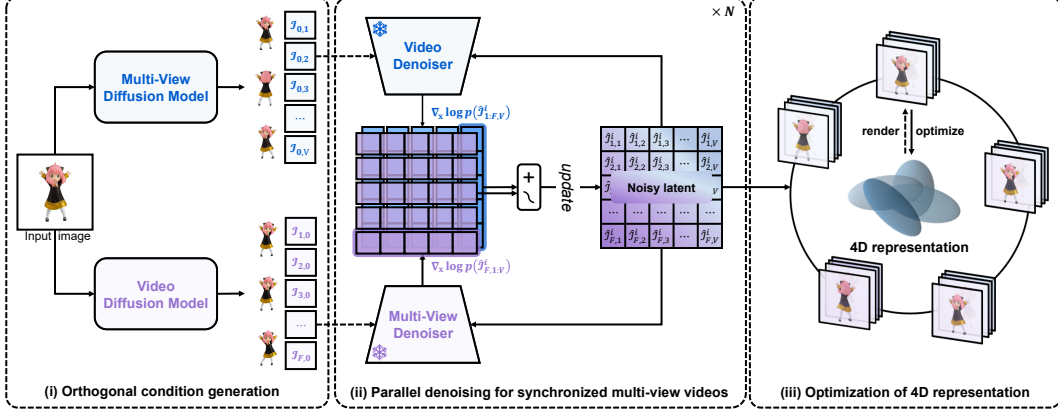


Figure 2: The overall pipeline of *Diffusion*<sup>2</sup>. **(i)** Given a reference image, *Diffusion*<sup>2</sup> first independently generates the animation under the reference view (denoted  $\mathcal{I}_{1:V,0}$ ) and the multi-view images at the reference time (denoted  $\mathcal{I}_{0,1:F}$ ) as the condition for the subsequent generation of the full matrix, denoted  $\mathcal{I}$ . Depending on the type of given prompt, the condition images  $\mathcal{I}_{1:V,0}$  or  $\mathcal{I}_{0,1:F}$  can be specified by users. **(ii)** Then, *Diffusion*<sup>2</sup> directly samples a dense multi-frame multi-view image array by blending the estimated scores with a weighting scheduler from pretrained video and multi-view diffusion models in the reverse diffusion process. **(iii)** The generated image arrays are employed as supervision to optimize a continuous 4D content representation.

$$\mathcal{I} = \{I_{i,j} \in \mathbb{R}^{H \times W \times 3}\}_{i=1,j=1}^{V,F} = \begin{bmatrix} I_{1,1} & \cdots & I_{1,j} & \cdots & I_{1,F} \\ \vdots & \ddots & \vdots & \ddots & \vdots \\ I_{i,1} & \cdots & I_{i,j} & \cdots & I_{i,F} \\ \vdots & \ddots & \vdots & \ddots & \vdots \\ I_{V,1} & \cdots & I_{V,j} & \cdots & I_{V,F} \end{bmatrix}, \quad (1)$$

where  $V$  is the number of views,  $F$  is the number of video frames, and  $(H, W)$  is the size of images. We aim to construct a generative model that allows us to directly sample natural  $\mathcal{I} \sim p(\mathcal{I})$ .

Now, let us first divert our focus to reviewing existing diffusion-based generators for video and multi-view images, which can be utilized for sampling realistic image sequence through the probabilistic flow ODE as below:

$$dx = -\dot{\sigma}(t)\sigma(t)\nabla_x \log p(x; \sigma(t)) dt. \quad (2)$$

Here,  $x = \{I_i \in \mathbb{R}^{H \times W \times 3}\}_{i=1}^N$  is a series of images with  $N$  frames or  $N$  views,  $\nabla_x \log p(x; \sigma)$  is the score function, which can be estimated as  $\nabla_x \log p(x; \sigma) \approx (D_\theta(x; \sigma)) / \sigma^2$  [18, 3], where  $D_\theta(x; \sigma)$  is a neural network trained via denoising score matching.

We want to extend the above formulation to the sampling of  $\mathcal{I}$ . The question is, how do we estimate the score of the joint distribution of  $V \times F$  images?

For clarity, denote  $\mathcal{I}_{-i,j} \triangleq \{I_{i',j} | 1 \leq i' \leq V, i' \neq i\}$ ,  $\mathcal{I}_{i,-j} \triangleq \{I_{i,j'} | 1 \leq j' \leq F, j' \neq j\}$  and  $\mathcal{I}_{-i,-j} \triangleq \{I_{i',j'} | 1 \leq i' \leq V, 1 \leq j' \leq F, i' \neq i, j' \neq j\}$ . We first make an assumption on the structure of  $p(\mathcal{I})$ .

**Assumption 3.1.** Given any image  $I_{i,j}$ , the underlying geometry  $I_{i',j} \in \mathcal{I}_{-i,j}$  and the dynamics  $I_{i,j'} \in \mathcal{I}_{i,-j}$  are conditionally independent, i.e.,

$$p(I_{i',j}, I_{i,j'} | I_{i,j}) = p(I_{i',j} | I_{i,j}) p(I_{i,j'} | I_{i,j}). \quad (3)$$

The assumption 3.1 implies that, given the front view at now of a 3D object, what its front view looks like in the future (or past) does not correlate with what the back view looks like now, which aligns with our intuition. Actually, assumption 3.1 is too strong to hold for some specific cases, yet this does not violate the correctness of our main theorem. For the conciseness and readability of the main text, we leave the discussion of the scope of the assumption and a more rigorous proof in Section A.3.

A natural corollary is that the mollified distribution derived by adding Gaussian noise into the data distribution still maintains conditional independence:



**Corollary 3.1.** Denote  $\hat{\mathcal{I}}$  as the noisy version of  $\mathcal{I}$ , i.e.,

$$\hat{\mathcal{I}} = \{\hat{I}_{i,j} \in \mathbb{R}^{H \times W \times 3}\}_{i=1,j=1}^{V,F} \quad \text{with } \hat{I}_{i,j} = \alpha I_{i,j} + \varepsilon_{i,j}, \quad (4)$$

where  $\alpha \in \mathbb{R}$  is a constant and  $\varepsilon_{i,j} \in \mathbb{R}^{H \times W \times 3}$  are independent Gaussian noises. Then equation (3) also holds for  $\hat{\mathcal{I}}$ .

This nice property allows us to sample the desired image matrix by progressively denoising from pure Gaussian noise using the combination of two estimated scores for its column and row, which can be obtained from the pretrained video and multi-view diffusion models respectively. Therefore, we can establish our main theorem.

**Theorem 3.1.** For  $\mathbf{x} = \hat{I}_{i,j}$ , we have

$$\nabla_{\mathbf{x}} \log p(\hat{\mathcal{I}}) = \nabla_{\mathbf{x}} \log p(\hat{\mathcal{I}}_{\{1:V\},j}) + \nabla_{\mathbf{x}} \log p(\hat{\mathcal{I}}_{i,\{1:F\}}) - \nabla_{\mathbf{x}} \log p(\hat{I}_{i,j}). \quad (5)$$

*Proof.* We first decompose  $p(\hat{\mathcal{I}})$  by

$$p(\hat{\mathcal{I}}) = p(\hat{I}_{i,j}, \hat{\mathcal{I}}_{-i,j}, \hat{\mathcal{I}}_{i,-j}, \hat{\mathcal{I}}_{-i,-j}) = p(\hat{I}_{i,j}, \hat{\mathcal{I}}_{-i,-j} | \hat{\mathcal{I}}_{-i,j}, \hat{\mathcal{I}}_{i,-j}) p(\hat{\mathcal{I}}_{-i,j}, \hat{\mathcal{I}}_{i,-j}). \quad (6)$$

Note that  $\forall \hat{I}_{i',j'} \in \hat{\mathcal{I}}_{-i,-j}$ ,  $I_{i',j'}$  and  $I_{i,j}$  are independent conditioned on  $I_{i',j}$  by corollary 3.1, hence

$$p(\hat{I}_{i,j}, \hat{\mathcal{I}}_{-i,-j} | \hat{\mathcal{I}}_{-i,j}, \hat{\mathcal{I}}_{i,-j}) = p(\hat{\mathcal{I}}_{-i,-j} | \hat{\mathcal{I}}_{-i,j}, \hat{\mathcal{I}}_{i,-j}) p(\hat{I}_{i,j} | \hat{\mathcal{I}}_{-i,j}, \hat{\mathcal{I}}_{i,-j}). \quad (7)$$

Since  $p(\hat{\mathcal{I}}_{-i,-j} | \hat{\mathcal{I}}_{-i,j}, \hat{\mathcal{I}}_{i,-j})$  does not contain  $\mathbf{x} (=I_{i,j})$ , its derivative with respect to  $\mathbf{x}$  is zero thus this term does not contribute to the score of  $I_{i,j}$ . Then combined with equation (6) and equation (7), taking the derivative of  $\log p(\hat{\mathcal{I}})$  with respect to  $\mathbf{x}$ , we achieve

$$\begin{aligned} \nabla_{\mathbf{x}} \log p(\hat{\mathcal{I}}) &= \nabla_{\mathbf{x}} \log p(\hat{I}_{i,j} | \hat{\mathcal{I}}_{-i,j}, \hat{\mathcal{I}}_{i,-j}) p(\hat{\mathcal{I}}_{-i,j}, \hat{\mathcal{I}}_{i,-j}) \\ &= \nabla_{\mathbf{x}} \log p(\hat{I}_{i,j}, \hat{\mathcal{I}}_{-i,j}, \hat{\mathcal{I}}_{i,-j}). \end{aligned} \quad (8)$$

Finally, by further decomposing  $p(\hat{I}_{i,j}, \hat{\mathcal{I}}_{-i,j}, \hat{\mathcal{I}}_{i,-j})$  and directly applying corollary 3.1, we obtain

$$\begin{aligned} \nabla_{\mathbf{x}} \log p(\hat{\mathcal{I}}) &= \nabla_{\mathbf{x}} \log p(\hat{\mathcal{I}}_{-i,j}, \hat{\mathcal{I}}_{i,-j} | \hat{I}_{i,j}) p(\hat{I}_{i,j}) \\ &= \nabla_{\mathbf{x}} \log p(\hat{\mathcal{I}}_{-i,j} | \hat{I}_{i,j}) p(\hat{\mathcal{I}}_{i,-j} | \hat{I}_{i,j}) p(\hat{I}_{i,j}) \\ &= \nabla_{\mathbf{x}} \log \frac{p(\hat{\mathcal{I}}_{\{1:V\},j}) p(\hat{\mathcal{I}}_{i,\{1:F\}})}{p(\hat{I}_{i,j})} \\ &= \nabla_{\mathbf{x}} \log p(\hat{\mathcal{I}}_{\{1:V\},j}) + \nabla_{\mathbf{x}} \log p(\hat{\mathcal{I}}_{i,\{1:F\}}) - \nabla_{\mathbf{x}} \log p(\hat{I}_{i,j}). \quad \square \end{aligned} \quad (9)$$

Here  $\nabla_{\mathbf{x}} \log p(\hat{\mathcal{I}}_{i,\{1:F\}})$  and  $\nabla_{\mathbf{x}} \log p(\hat{\mathcal{I}}_{\{1:V\},j})$  are just the score functions of the video diffusion model and the multi-view diffusion model respectively. Since the  $\nabla_{\mathbf{x}} \log p(\hat{I}_{i,j})$  is intractable in the conditional generation, we use the convex combination of  $\nabla_{\mathbf{x}} \log p(\hat{\mathcal{I}}_{i,\{1:F\}})$  and  $\nabla_{\mathbf{x}} \log p(\hat{\mathcal{I}}_{\{1:V\},j})$  to replace it as:

$$\nabla_{\mathbf{x}} \log p(\hat{I}_{i,j}) = (1-s) \nabla_{\mathbf{x}} \log p(\hat{\mathcal{I}}_{i,\{1:F\}}) + s \nabla_{\mathbf{x}} \log p(\hat{\mathcal{I}}_{\{1:V\},j}). \quad (10)$$

In practice, we employ a logistic schedule to adjust  $s$  at each denoising step. Given the current denoising step  $i$  and the number of total steps  $N$ , we set  $s = 1 - \frac{1}{1 + e^{k(i/N - s_0)}}$ . This function has a sigmoidal curve, which is relatively flat at the extremes away from middle  $s_0$  and changes sharply near it, with the derivative controlled by  $k$ . This schedule decouples the generation of consistent geometry and temporally smooth appearance to some extent.

**Sampling in latent space** For convenience, the above theorem assumes that we sample images in RGB space. However, modern high-resolution diffusion models typically generate images in a latent space encoded by pretrained auto-encoder [20, 41]. The legitimacy of the aforementioned derivation requires that the multi-view generator and the video generator share the same latent space. This requirement is not met by most existing instantiation of them. However, as pointed out by SVD [3], video generation models trained on large-scale video datasets have learned a strong stereo knowledge, thus providing a better pretraining for multi-view diffusion models than those trained solely on image data. Therefore, we believe that the requirement will be increasingly satisfied in the future.

**Generation with various input conditions** Note that the formulation described above is based on unconditional generation. However, we are more interested in controllable generation in practice. Then we will discuss on how to extend the above process to conditional generation. Consider the augmented matrix  $\mathcal{I}_{\text{aug}}$  defined by

$$\mathcal{I}_{\text{aug}} = \begin{bmatrix} I_{0,0} & \mathcal{I}_{0,\{1:V\}} \\ \mathcal{I}_{\{1:F\},0} & \mathcal{I} \end{bmatrix}. \quad (11)$$

Compared to the aforementioned unconditional generation, the augmented matrix  $\mathcal{I}_{\text{aug}}$  additionally includes the optional input image  $I_{0,0}$ , and  $\mathcal{I}_{0,\{1:V\}}$ ,  $\mathcal{I}_{\{1:F\},0}$  that represent the reference geometry and dynamic of target object. To incorporate them into the generation of  $\mathcal{I}$ , we condition the score estimator for denoising each row (or column) in equations (5) and (10) on the first element of the same row (or column) in  $\mathcal{I}_{\text{aug}}$ . This formulation enables us to handle various 4D generation tasks depending on different forms of conditions specified by users as below:

- **Image-to-4D.** Given  $I_{0,0}$  as input, both  $\mathcal{I}_{0,\{1:V\}}$  and  $\mathcal{I}_{\{1:F\},0}$  are generated by diffusion models.
- **Video-to-4D.** Given  $\mathcal{I}_{\{0:F\},0}$  as input, we use the last frame  $I_{0,0}$  as the condition of multi-view diffusion model to generate  $\mathcal{I}_{0,\{1:V\}}$ .
- **3D-to-4D.** Similarly, Given  $\mathcal{I}_{0,\{0:V\}}$  as input, we use the front view  $I_{0,0}$  as the condition of video diffusion model to generate  $\mathcal{I}_{\{1:F\},0}$ .
- **Text-to-4D.** The above inputs including single image  $I_{0,0}$ , single-view video  $\mathcal{I}_{\{0:F\},0}$  and static multi-view images  $\mathcal{I}_{0,\{0:V\}}$  can all be generated guided by text.

Once  $\mathcal{I}_{0,\{1:V\}}$ ,  $\mathcal{I}_{\{1:F\},0}$  are obtained, we can sample the full matrix  $\mathcal{I}$  using equations (5) and (10).

**Parallel denoising** Assumption 3.1 ensures the safety of independently generating the geometry  $\mathcal{I}_{0,\{1:V\}}$  and the motion  $\mathcal{I}_{\{1:F\},0}$ . Since these two generation processes have no computational or data dependency, their total time cost could be reduced to a single reverse diffusion process. Additionally, when we denoise the rest part of  $\mathcal{I}_{\text{aug}}$ , *i.e.*,  $\mathcal{I}$ , the score estimation for each row and column can also be parallelized in each denoising step. Therefore, with sufficient GPU memory, the total time spent on the process illustrated in Figure 2 (ii) remains the same as that for generating a single video.

### 3.2 Robust reconstruction

**4D representation** Given generated synchronized multi-view videos from any type of condition, there are numerous methods that can be employed to reconstruct complete 4D assets. Among these candidates, we adopt the 4D Gaussian Splatting [50] due to its superior fitting capabilities and efficient optimization given the dense multi-view supervision.

**Optimization** Although the images produced in the first stage already exhibit intuitively satisfactory spatiotemporal consistency, the performance limitation of the foundational diffusion model still makes it difficult to achieve precise pixel-level matching across different views and frames. Therefore, we follow [7] to optimize the combination of perception loss  $\mathcal{L}_{l_{\text{lips}}}$  [56] and D-SSIM  $\mathcal{L}_{ssim}$  [46] while discarding L1 loss. In addition, we weight each term with the confidence score as [28], then the total objective is defined as  $\mathcal{L}_{\text{total}} = \lambda_{l_{\text{lips}}} \mathcal{C}_{l_{\text{lips}}} \mathcal{L}_{l_{\text{lips}}} + \lambda_{ssim} \mathcal{C}_{ssim} \mathcal{L}_{ssim}$ , where  $\mathcal{C}_{ssim}$  is just the SSIM between ground truth and rendered images and  $\mathcal{C}_{l_{\text{lips}}}$  is defined as  $1 - \mathcal{L}_{l_{\text{lips}}}$ .

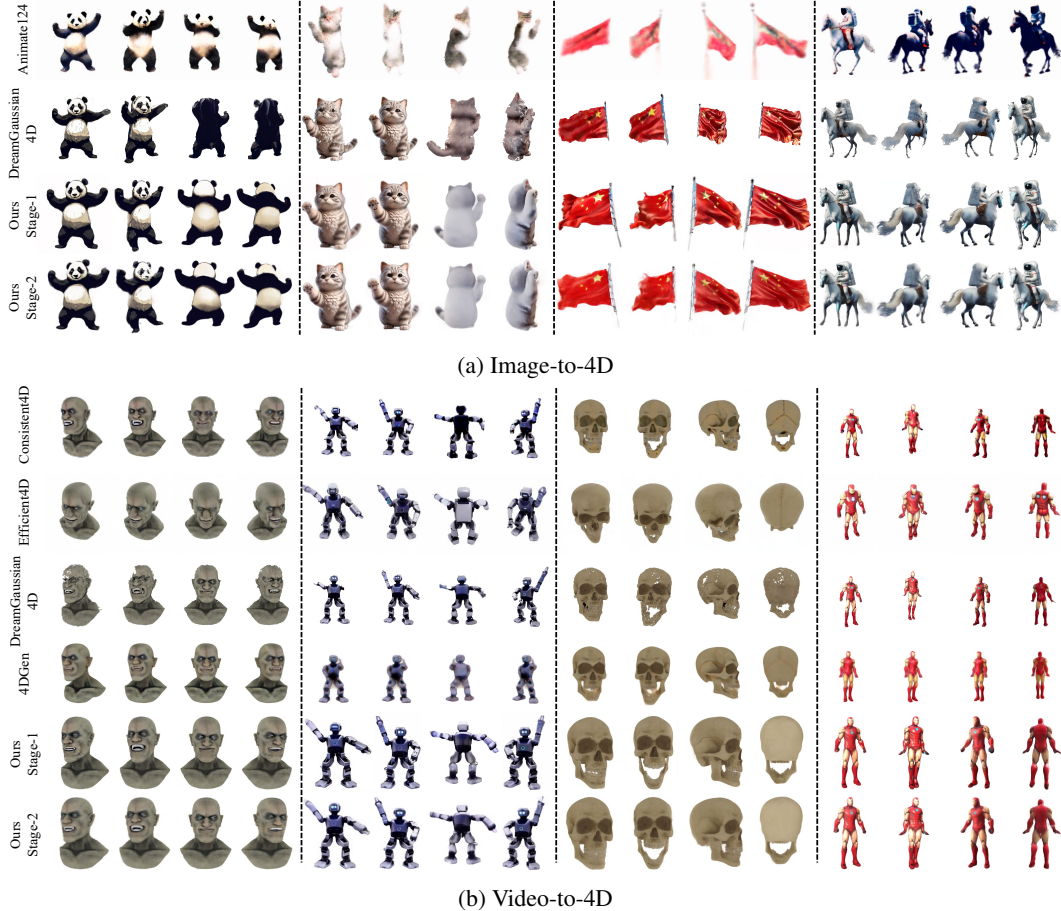


Figure 3: **Qualitative comparisons** on (a) image-to-4D generation and (b) video-to-4D generation.

## 4 Experiments

### 4.1 Implementation details

In the first stage, we employ Stable Video Diffusion [3] as our foundation video diffusion model, predicting 25 frames each time conditioning on the reference image. SV3D<sup>P</sup> [42] is chosen as our foundation multi-view diffusion model. For simplicity, we only generate orbital videos with 21 uniformly spaced azimuths and fixed elevation while manually filtering out side views as these views typically contain thin structures that pose challenges for the video generation model and subsequent reconstruction processes. By default, we set the number of sampling steps to 50 for both models. In the reconstruction stage, we assume that the virtual camera whose FOV is set to 33.8° orbiting around the object center with a fixed radius of 2m to align with the training data of SV3D. Finally, We optimized 4D Gaussian Splatting for 5,000 iterations without bells and whistles. The image size is set to (576 × 576) in both stages. All the experiments are conducted on eight NVIDIA A6000 GPUs. Please refer to Section A.4 for more details.

### 4.2 Main results

**4D generation from reference image** In Figure 3 (a), we present the results generated by our method and compare them with other alternatives. It can be observed that our simple and elegant pipeline is capable of generating 4D assets with comparable quality to those produced by SDS-based methods using sophisticated multi-stage optimization. Furthermore, the parallel denoising characteristic can provide an efficiency advantage for our method over those need recurrent evaluation of diffusion UNet. We also conducted a user study in Table 1. It suggests that our method garnered the highest preference in the multi-view consistency, detail, and overall model quality.

Table 1: **User study** on image-to-4D generation. The proportions of different methods that best match user preferences under three criteria are reported.

Method	Details	Geometrical consistency	Temporal smoothness	Overall model quality	Generation time
Animate124 [57]	11.3%	31.0%	16.0%	18.0%	9h
DreamGaussian4D [31]	27.7%	24.3%	<b>48.0%</b>	25.7%	12m
<i>Diffusion</i> <sup>2</sup> (Ours)	<b>61.0%</b>	<b>44.7%</b>	36.0%	<b>56.3%</b>	<b>10m</b>

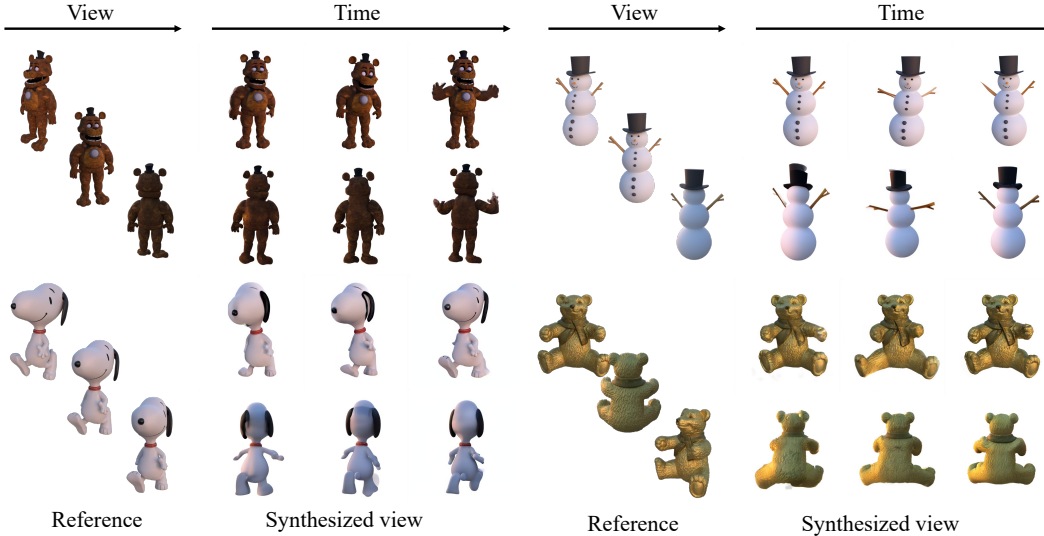


Figure 4: Synthesized images from static 3D models.

Table 2: Quantitative comparisons on video-to-4D generation.

Method	Type	CLIP Similarity $\uparrow$	Generation time $\downarrow$
Consistent4D [16]	Optimization-based	0.87	2h
4DGen [53]	Optimization-based	0.89	2h10m
Efficient4D [28]	Photogrammetry-based	0.92	14m
<i>Diffusion</i> <sup>2</sup> (Ours)	Photogrammetry-based	<b>0.94</b>	<b>10m</b>

**4D generation from single view video** Generating 4D dynamic objects from single-view video is a practical task first introduced in [16]. Compared to image-to-4D generation, this task places additional constraints on the object’s motion. Our proposed framework can be easily adapted to deal with this task as detailed in Section 3.1. We perform both quantitative and qualitative comparisons with other counterparts in this setting. The qualitative result is shown in Figure 3 (b). It can be seen that our method slightly reduces the over-saturated appearance led by SDS while achieving more clear details. For quantitative evaluation, we report the CLIP-similarity between generated views and ground truth images to indicate overall semantic consistency and the recognizability of generated images. As shown in Table 2, our method can achieve better CLIP similarity than other alternatives.

**4D generation from static 3D content** Naturally, *Diffusion*<sup>2</sup> can also animate static 3D models as described in Section 3.1, which has substantial practical implications. From Figure 4 we can observe that our method is capable of endowing 3D models with diverse and realistic dynamics while maintaining satisfactory temporal and geometrical consistency. More results including text-to-4D can be found in Section A.5.

### 4.3 Ablation studies

Since previous methods have explored dynamic content reconstruction well, we mainly focus on the ablation of key design choices in the stage of image matrix generation. Recall that in equation (10), we use  $s$  to balance the contribution of two foundation models. And we choose a logistic function

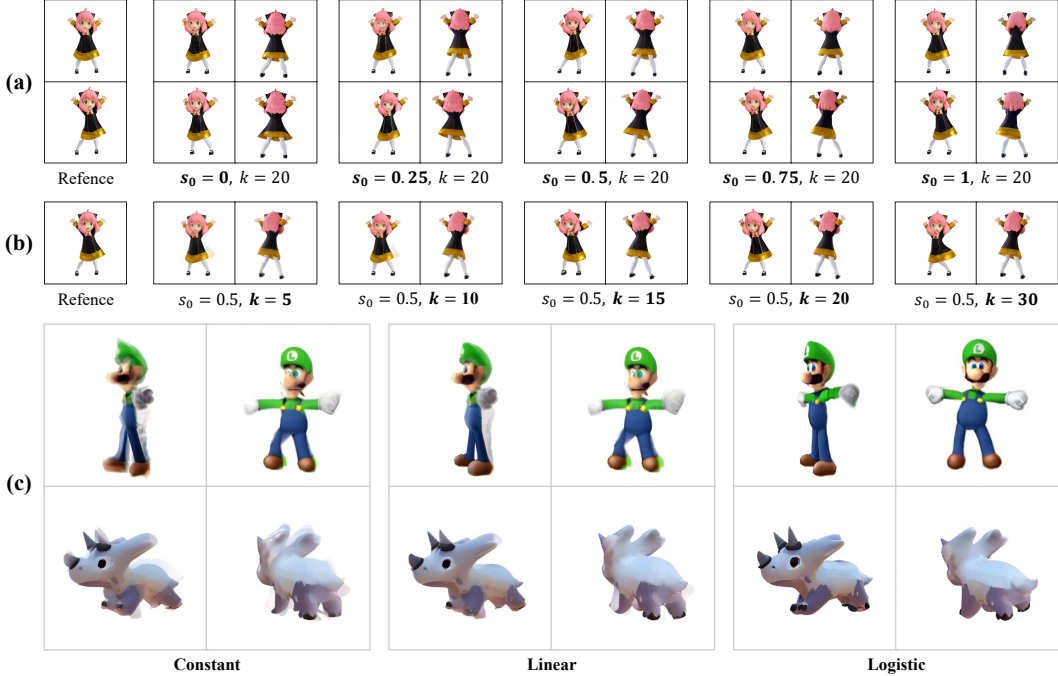


Figure 5: **Ablation studies.** (a) & (b) The tuning of parameters  $s_0$  and  $k$  controlling the logistic schedule. (c) Different types of scale schedule. Best viewed with zoom-in.

$s = 1 - \frac{1}{1 + e^{k(i/N - s_0)}}$  as the schedule of  $s$ , which has two hyper-parameters  $s_0$  and  $k$  controlling the shape of the function. Then we tune  $s_0$  and  $k$  to study their impact on generation.

**Impact of  $s_0$**  In Figure 5 (a), we tune  $s_0$  with  $k$  fixed to 20. We first consider two extreme cases. In the first case, we set  $s_0 = 0$ , implying that  $s < 0.5$  all the time and SVD has dominant contribution in equation (5). As shown in “ $s_0 = 0, k = 20$ ” of Figure 5 (a), the dress still evenly sags down both sides of the body, unlike in the reference view where the dress flutters to the left side of the body. This indicates that without the sufficient guidance of geometry prior, the dynamics of each view will be independent of each other. Another extreme is when we set  $s_0 = 1$ , where SV3D has dominant contribution. In this case, it can no longer guarantee the consistency of details between different frames of invisible views. The comparison of the images of “ $s_0 = 1, k = 20$ ” shows a remarkable change in the shape of the tail of the hair. By further telescoping the results with different  $s_0$ , we finally adopt a compromised option to set  $s_0$  to 0.5, *i.e.*, starting to drastically reduce the weight of the multi-view score at halfway of the denoising process. In most cases, this choice can achieve a satisfactory trade-off between smooth temporal transitions and geometrical consistency.

**Impact of  $k$**  In addition, the decreasing speed of  $s_0$  may also affect the quality of generated images, which is controlled by another parameter  $k$ . Therefore, we test the image generation under different  $k$  given  $s_0 = 0.5$  in Figure 5 (b). It can be seen that when  $k$  is relatively small, the generated images may exhibit ghosting effects. On the other hand, when  $k$  is too large, it may weaken the temporal smoothing effect brought by the video diffusion model in the early stage of denoising process. Consequently, we adopt  $s = 0.5, k = 20$  as the default setting.

**Impact of logistic schedule** Finally, we also examined the impact of different schedule types, as shown in Figure 5 (c). We compare with two counterparts: “Constant” ( $s \equiv 0.5$ ) and “Linear” ( $s = \frac{i}{N}$ ). It can be observed that other alternates would lead to ghosting artifacts.

## 5 Conclusion

In this work, we introduce *Diffusion*<sup>2</sup>, a novel framework for creating dynamic 3D content. This framework first generates a dense array of multi-view and multi-frame images with high parallelization, which are then used to build a full 4D representation through a reconstruction pipeline. The core assumption behind this framework is that the motion of an object viewed from one angle and its



appearance from another are conditionally independent. Based on this assumption, we prove that we can directly sample synchronized multi-view videos in a denoising process by combining pretrained video and multi-view diffusion models. Our experimental results demonstrate the flexibility and effectiveness of our framework, showing that it can adapt to various prompts to produce high-quality 4D content efficiently and effectively. We hope that our work can inspire future research on unleashing and combining the geometrical and dynamic priors from foundation 3D and video diffusion models.

## References

- [1] Sherwin Bahmani, Ivan Skorokhodov, Victor Rong, Gordon Wetzstein, Leonidas Guibas, Peter Wonka, Sergey Tulyakov, Jeong Joon Park, Andrea Tagliasacchi, and David B Lindell. 4d-fy: Text-to-4d generation using hybrid score distillation sampling. In *CVPR*, 2024. 1, 3
- [2] Omer Bar-Tal, Lior Yariv, Yaron Lipman, and Tali Dekel. Multidiffusion: Fusing diffusion paths for controlled image generation. In *ICML*, 2023. 2
- [3] Andreas Blattmann, Tim Dockhorn, Sumith Kulal, Daniel Mendelevitch, Maciej Kilian, Dominik Lorenz, Yam Levi, Zion English, Vikram Voleti, Adam Letts, et al. Stable video diffusion: Scaling latent video diffusion models to large datasets. *arXiv preprint*, 2023. 2, 3, 4, 6, 7
- [4] Andreas Blattmann, Robin Rombach, Huan Ling, Tim Dockhorn, Seung Wook Kim, Sanja Fidler, and Karsten Kreis. Align your latents: High-resolution video synthesis with latent diffusion models. In *CVPR*, 2023. 2, 3
- [5] Tim Brooks, Bill Peebles, Connor Holmes, Will DePue, Yufei Guo, Li Jing, David Schnurr, Joe Taylor, Troy Luhman, Eric Luhman, Clarence Ng, Ricky Wang, and Aditya Ramesh. Video generation models as world simulators. <https://openai.com/research/video-generation-models-as-world-simulators>, 2024. 2, 3
- [6] Anpei Chen, Zexiang Xu, Andreas Geiger, Jingyi Yu, and Hao Su. Tensorf: Tensorial radiance fields. In *ECCV*, 2022. 1
- [7] Zilong Chen, Yikai Wang, Feng Wang, Zhengyi Wang, and Huaping Liu. V3d: Video diffusion models are effective 3d generators. *arXiv preprint*, 2024. 1, 3, 6
- [8] Matt Deitke, Dustin Schwenk, Jordi Salvador, Luca Weihs, Oscar Michel, Eli VanderBilt, Ludwig Schmidt, Kiana Ehsani, Aniruddha Kembhavi, and Ali Farhadi. Objaverse: A universe of annotated 3d objects. In *CVPR*, 2023. 1, 3, 15
- [9] Yuanxing Duan, Fangyin Wei, Qiyu Dai, Yuhang He, Wenzheng Chen, and Baoquan Chen. 4d gaussian splatting: Towards efficient novel view synthesis for dynamic scenes. *arXiv preprint*, 2024. 1
- [10] Jun Gao, Tianchang Shen, Zian Wang, Wenzheng Chen, Kangxue Yin, Daiqing Li, Or Litany, Zan Gojcic, and Sanja Fidler. Get3d: A generative model of high quality 3d textured shapes learned from images. In *NeurIPS*, 2022. 3
- [11] Quankai Gao, Qiangeng Xu, Zhe Cao, Ben Mildenhall, Wenchao Ma, Le Chen, Danhang Tang, and Ulrich Neumann. Gaussianflow: Splatting gaussian dynamics for 4d content creation. *arXiv preprint*, 2024. 1
- [12] Agrim Gupta, Lijun Yu, Kihyuk Sohn, Xiuye Gu, Meera Hahn, Li Fei-Fei, Irfan Essa, Lu Jiang, and José Lezama. Photorealistic video generation with diffusion models. *arXiv preprint*, 2023. 3
- [13] Junlin Han, Filippos Kokkinos, and Philip Torr. Vfusion3d: Learning scalable 3d generative models from video diffusion models. *arXiv preprint*, 2024. 3
- [14] Jonathan Ho, Ajay Jain, and Pieter Abbeel. Denoising diffusion probabilistic models. In *NeurIPS*, 2020. 1, 3
- [15] Yicong Hong, Kai Zhang, Jiuxiang Gu, Sai Bi, Yang Zhou, Difan Liu, Feng Liu, Kalyan Sunkavalli, Trung Bui, and Hao Tan. Lrm: Large reconstruction model for single image to 3d. In *ICLR*, 2024. 1, 3
- [16] Yanqin Jiang, Li Zhang, Jin Gao, Weimin Hu, and Yao Yao. Consistent4d: Consistent 360° dynamic object generation from monocular video. In *ICLR*, 2024. 1, 2, 3, 8, 15, 17
- [17] Heewoo Jun and Alex Nichol. Shap-e: Generating conditional 3d implicit functions. *arXiv preprint*, 2023. 3

- [18] Tero Karras, Miika Aittala, Timo Aila, and Samuli Laine. Elucidating the design space of diffusion-based generative models. In *NeurIPS*, 2022. 1, 4
- [19] Bernhard Kerbl, Georgios Kopanas, Thomas Leimkühler, and George Drettakis. 3d gaussian splatting for real-time radiance field rendering. In *ACM TOG*, 2023. 1
- [20] Diederik P Kingma and Max Welling. Auto-encoding variational bayes. In *ICLR*, 2014. 6
- [21] Yuseung Lee, Kunho Kim, Hyunjin Kim, and Minhyuk Sung. Syncdiffusion: Coherent montage via synchronized joint diffusions. In *NeurIPS*, 2023. 2
- [22] Ruoshi Liu, Rundi Wu, Basile Van Hoorick, Pavel Tokmakov, Sergey Zakharov, and Carl Vondrick. Zero-1-to-3: Zero-shot one image to 3d object. In *ICCV*, 2023. 1, 3, 17
- [23] Yuan Liu, Cheng Lin, Zijiao Zeng, Xiaoxiao Long, Lingjie Liu, Taku Komura, and Wenping Wang. Syncdreamer: Generating multiview-consistent images from a single-view image. In *ICLR*, 2024. 1, 2, 3
- [24] Xiaoxiao Long, Yuan-Chen Guo, Cheng Lin, Yuan Liu, Zhiyang Dou, Lingjie Liu, Yuexin Ma, Song-Hai Zhang, Marc Habermann, Christian Theobalt, et al. Wonder3d: Single image to 3d using cross-domain diffusion. *arXiv preprint*, 2023. 3
- [25] Haoyu Lu, Guoxing Yang, Nanyi Fei, Yuqi Huo, Zhiwu Lu, Ping Luo, and Mingyu Ding. Vdt: General-purpose video diffusion transformers via mask modeling. In *ICLR*, 2024. 3
- [26] Alex Nichol, Heewoo Jun, Pratul Dharwal, Pamela Mishkin, and Mark Chen. Point-e: A system for generating 3d point clouds from complex prompts. *arXiv preprint*, 2022. 3
- [27] Zijie Pan, Jiachen Lu, Xiatian Zhu, and Li Zhang. Enhancing high-resolution 3d generation through pixel-wise gradient clipping. In *ICLR*, 2024. 3
- [28] Zijie Pan, Zeyu Yang, Xiatian Zhu, and Li Zhang. Fast dynamic 3d object generation from a single-view video. *arXiv preprint*, 2024. 3, 6, 8
- [29] Ben Poole, Ajay Jain, Jonathan T Barron, and Ben Mildenhall. Dreamfusion: Text-to-3d using 2d diffusion. In *ICLR*, 2023. 1, 3
- [30] Jeremy Reizenstein, Roman Shapovalov, Philipp Henzler, Luca Sbordone, Patrick Labatut, and David Novotny. Common objects in 3d: Large-scale learning and evaluation of real-life 3d category reconstruction. In *ICCV*, 2021. 1
- [31] Jiawei Ren, Liang Pan, Jiayang Tang, Chi Zhang, Ang Cao, Gang Zeng, and Ziwei Liu. Dreamgaussian4d: Generative 4d gaussian splatting. *arXiv preprint*, 2023. 1, 2, 3, 8
- [32] Robin Rombach, Andreas Blattmann, Dominik Lorenz, Patrick Esser, and Björn Ommer. High-resolution image synthesis with latent diffusion models. In *CVPR*, 2022. 3
- [33] Katja Schwarz, Yiyi Liao, Michael Niemeyer, and Andreas Geiger. Graf: Generative radiance fields for 3d-aware image synthesis. In *NeurIPS*, 2020. 3
- [34] Yichun Shi, Peng Wang, Jianglong Ye, Mai Long, Kejie Li, and Xiao Yang. Mvdream: Multi-view diffusion for 3d generation. *arXiv preprint*, 2023. 1, 3
- [35] Uriel Singer, Shelly Sheynin, Adam Polyak, Oron Ashual, Iurii Makarov, Filippos Kokkinos, Naman Goyal, Andrea Vedaldi, Devi Parikh, Justin Johnson, et al. Text-to-4d dynamic scene generation. *arXiv preprint*, 2023. 1, 3
- [36] Jiaming Song, Chenlin Meng, and Stefano Ermon. Denoising diffusion implicit models. In *ICLR*, 2021. 1
- [37] Yang Song, Jascha Sohl-Dickstein, Diederik P Kingma, Abhishek Kumar, Stefano Ermon, and Ben Poole. Score-based generative modeling through stochastic differential equations. In *ICLR*, 2021. 1
- [38] Jiayang Tang, Zhaoxi Chen, Xiaokang Chen, Tengfei Wang, Gang Zeng, and Ziwei Liu. Lgm: Large multi-view gaussian model for high-resolution 3d content creation. *arXiv preprint*, 2024. 1, 3
- [39] Jiayang Tang, Jiawei Ren, Hang Zhou, Ziwei Liu, and Gang Zeng. Dreamgaussian: Generative gaussian splatting for efficient 3d content creation. In *ICLR*, 2024. 1, 3

- [40] Shitao Tang, Jiacheng Chen, Dilin Wang, Chengzhou Tang, Fuyang Zhang, Yuchen Fan, Vikas Chandra, Yasutaka Furukawa, and Rakesh Ranjan. Mvdifffusion++: A dense high-resolution multi-view diffusion model for single or sparse-view 3d object reconstruction. *arXiv preprint*, 2024. 1, 2, 3
- [41] Aaron Van Den Oord, Oriol Vinyals, et al. Neural discrete representation learning. In *NeurIPS*, 2017. 6
- [42] Vikram Voleti, Chun-Han Yao, Mark Boss, Adam Letts, David Pankratz, Dmitry Tochilkin, Christian Laforte, Robin Rombach, and Varun Jampani. Sv3d: Novel multi-view synthesis and 3d generation from a single image using latent video diffusion. *arXiv preprint*, 2024. 1, 2, 3, 7
- [43] Peng Wang and Yichun Shi. Imagedream: Image-prompt multi-view diffusion for 3d generation. *arXiv preprint*, 2023. 1, 3
- [44] Zhengyi Wang, Cheng Lu, Yikai Wang, Fan Bao, Chongxuan Li, Hang Su, and Jun Zhu. Prolificdreamer: High-fidelity and diverse text-to-3d generation with variational score distillation. In *NeurIPS*, 2023. 1, 3
- [45] Zhengyi Wang, Yikai Wang, Yifei Chen, Chendong Xiang, Shuo Chen, Dajiang Yu, Chongxuan Li, Hang Su, and Jun Zhu. Crm: Single image to 3d textured mesh with convolutional reconstruction model. *arXiv preprint*, 2024. 3
- [46] Zhou Wang, Alan C Bovik, Hamid R Sheikh, and Eero P Simoncelli. Image quality assessment: from error visibility to structural similarity. In *IEEE TIP*, 2004. 6
- [47] Guanjun Wu, Taoran Yi, Jiemin Fang, Lingxi Xie, Xiaopeng Zhang, Wei Wei, Wenyu Liu, Qi Tian, and Xinggang Wang. 4d gaussian splatting for real-time dynamic scene rendering. In *CVPR*, 2024. 1
- [48] Tianxing Wu, Chenyang Si, Yuming Jiang, Ziqi Huang, and Ziwei Liu. Freeinit: Bridging initialization gap in video diffusion models. *arXiv preprint*, 2023. 15
- [49] Tong Wu, Jiarui Zhang, Xiao Fu, Yuxin Wang, Liang Pan Jiawei Ren, Wayne Wu, Lei Yang, Jiaqi Wang, Chen Qian, Dahua Lin, and Ziwei Liu. Omniobject3d: Large-vocabulary 3d object dataset for realistic perception, reconstruction and generation. In *CVPR*, 2023. 1
- [50] Zeyu Yang, Hongye Yang, Zijie Pan, and Li Zhang. Real-time photorealistic dynamic scene representation and rendering with 4d gaussian splatting. In *ICLR*, 2024. 6
- [51] Ziyi Yang, Xinyu Gao, Wen Zhou, Shaohui Jiao, Yuqing Zhang, and Xiaogang Jin. Deformable 3d gaussians for high-fidelity monocular dynamic scene reconstruction. In *CVPR*, 2024. 1, 3
- [52] Taoran Yi, Jiemin Fang, Guanjun Wu, Lingxi Xie, Xiaopeng Zhang, Wenyu Liu, Qi Tian, and Xinggang Wang. Gaussiandreamer: Fast generation from text to 3d gaussian splatting with point cloud priors. In *CVPR*, 2024. 3
- [53] Yuyang Yin, Dejie Xu, Zhangyang Wang, Yao Zhao, and Yunchao Wei. 4dgen: Grounded 4d content generation with spatial-temporal consistency. *arXiv preprint*, 2023. 2, 3, 8
- [54] Xianggang Yu, Mutian Xu, Yidan Zhang, Haolin Liu, Chongjie Ye, Yushuang Wu, Zizheng Yan, Chenming Zhu, Zhangyang Xiong, Tianyou Liang, et al. Mvimnet: A large-scale dataset of multi-view images. In *CVPR*, 2023. 1, 3
- [55] Lvmin Zhang, Anyi Rao, and Maneesh Agrawala. Adding conditional control to text-to-image diffusion models. In *ICCV*, 2023. 1
- [56] Richard Zhang, Phillip Isola, Alexei A Efros, Eli Shechtman, and Oliver Wang. The unreasonable effectiveness of deep features as a perceptual metric. In *CVPR*, 2018. 6
- [57] Yuyang Zhao, Zhiwen Yan, Enze Xie, Lanqing Hong, Zhenguo Li, and Gim Hee Lee. Animate124: Animating one image to 4d dynamic scene. *arXiv preprint*, 2023. 1, 8, 15
- [58] Qi Zuo, Xiaodong Gu, Lingteng Qiu, Yuan Dong, Zhengyi Zhao, Weihao Yuan, Rui Peng, Siyu Zhu, Zilong Dong, Liefeng Bo, et al. Videomv: Consistent multi-view generation based on large video generative model. *arXiv preprint*, 2024. 1

## A Appendix

### A.1 Discussions on the potential social impacts

In general, the proposed method has the potential to inspire a new approach to the automatic generation of dynamic 3D content. This could substantially lower the barriers to becoming an animator, save human resources within animation production, and ultimately reshape the industry’s landscape. Nonetheless, this transition may bring about issues such as unemployment and poverty for individuals whose livelihoods rely on these animation skills. Therefore, it may be necessary to gradually reduce the training scale in this industry and recalibrate the human resource supply to better align with the demands of future market.

On the other hand, the core contribution of *Diffusion*<sup>2</sup> lies in reducing the 4D generation problem to the reconciliation of video and multi-view diffusion models. This indeed allows us to leverage recent advancements in these active fields effectively. However, the racial, gender, and cultural biases and stereotypes inherent in the foundational models may also be introduced into the generated 4D assets. Additionally, the potential abuse of generative models which may lead to copyright issues is also a matter of concern.

### A.2 Limitations

As a preliminary exploration of zero-shot sampling of multi-view synchronized videos, this work still has some limitations. Overall, the performance of the proposed framework is severely constrained by the foundation generative models. For example, as can be seen from the second example in Figure 3 (a), the model has generated a weird textureless back for the cat. Additionally, due to biases in the training data of the video generation model, it is very unfriendly to thin structures in side views without clear semantics, easily generating unrealistic and inconsistent motions in these viewpoints. Furthermore, the motion generated by currently available video generation models may still be blurry or even corrupted. All these issues bring serious challenges to the subsequent reconstruction. However, we believe that the above problems will eventually be addressed with the further development of generative models, especially video generation models.

### A.3 The applicability of the assumption and proof for the theorem in general case

Another risk that needs to be pointed out is that our assumption about the conditional independence is too strong to apply in some cases. For example, if the target object rotates 180° over a period of time, the back view at the current moment and the front view after a period of time should not be conditionally independent given the front view at the current moment. However, existing video diffusion models typically generate videos from a single view without rotational movements, and our pipeline allows users to specify conditions to exclude such cases. Therefore, we have not discussed the potential limitations of this assumption in the main text for better readability and brevity of proof.

It is worth noting that, even in such cases that violate assumption 3.1, our method can still work well. This is because the main theorem remains valid under these case and its correctness does not essentially rely on such a strong assumption. Actually, although extreme rotations might exist when considering frames with large intervals, they are unlikely to occur between adjacent frames in a natural video. Now considering that the distribution of  $\hat{I}_{i,j}$  is almost entirely determined by its adjacent frames and views, we have the continuity assumption:

**Assumption A.1. (Continuity assumption)** Denote  $\hat{\mathcal{I}}_{i_{near},j} \in \hat{\mathcal{I}}_{-i,j}$ ,  $\hat{\mathcal{I}}_{i,j_{near}} \in \hat{\mathcal{I}}_{i,-j}$  are the views and frames close enough to  $\hat{I}_{i,j}$  to provide sufficient information for the distribution of it while keeping sufficiently continuous, then

$$p\left(\hat{I}_{i,j}|\hat{\mathcal{I}}_{-i,j}\right) \approx p\left(\hat{I}_{i,j}|\hat{\mathcal{I}}_{i_{near},j}\right) \quad (12)$$

$$p\left(\hat{I}_{i,j}|\hat{\mathcal{I}}_{i,-j}\right) \approx p\left(\hat{I}_{i,j}|\hat{\mathcal{I}}_{i,j_{near}}\right) \quad (13)$$

$$p\left(\hat{I}_{i,j}|\hat{\mathcal{I}}_{i_{near},j},\hat{\mathcal{I}}_{i,j_{near}},\hat{\mathcal{I}}_{i',j'}\right) \approx p\left(\hat{I}_{i,j}|\hat{\mathcal{I}}_{i_{near},j},\hat{\mathcal{I}}_{i,j_{near}}\right), \quad (14)$$

where  $\hat{I}_{i',j'} \notin \{\hat{I}_{i,j},\hat{\mathcal{I}}_{i_{near},j},\hat{\mathcal{I}}_{i,j_{near}}\}$ .

Further note that the near index is symmetric, *i.e.*, if  $\hat{I}_{i',j} \in \hat{I}_{i_{\text{near}},j}$ , then  $\hat{I}_{i,j} \in \hat{I}_{i',j}$ . Then we relax the assumption 3.1 as follows:

**Assumption A.2. (Weak version of assumption 3.1)** Given any image  $I_{i,j}$ , the nearby geometry  $I_{i',j} \in \mathcal{I}_{i_{\text{near}},j}$  and the nearby dynamics  $I_{i,j'} \in \mathcal{I}_{i,j_{\text{near}}}$  are conditionally independent, *i.e.*,

$$p(I_{i',j}, I_{i,j'} | I_{i,j}) = p(I_{i',j} | I_{i,j}) p(I_{i,j'} | I_{i,j}). \quad (15)$$

Similar condition also holds for  $\hat{\mathcal{I}}$ .

Finally, we can establish our main theorem 3.1 under the additional assumptions.

*Proof of theorem 3.1 under assumption A.1 and assumption A.2.*

Following the same derivation of the original proof 3.1, equations (6), (7) and (8) remain unchanged but all “=” in (7) and (8) should be “ $\approx$ ” because equation (7) is now established on equation (14) of assumption A.1 instead of assumption 3.1.

Then integrating new assumptions to correct equation (9), we obtain:

$$\begin{aligned} \nabla_x \log p(\hat{\mathcal{I}}) &\approx \nabla_x \log p(\hat{I}_{i,j} | \hat{\mathcal{I}}_{-i,j}, \hat{\mathcal{I}}_{i,-j}) p(\hat{\mathcal{I}}_{-i,j}, \hat{\mathcal{I}}_{i,-j}) \\ &= \nabla_x \log p(\hat{I}_{i,j} | \hat{\mathcal{I}}_{-i,j}, \hat{\mathcal{I}}_{i,-j}) + \underbrace{\nabla_x \log p(\hat{\mathcal{I}}_{-i,j}, \hat{\mathcal{I}}_{i,-j})}_{=0} \\ &\approx \nabla_x \log p(\hat{I}_{i,j} | \hat{\mathcal{I}}_{i_{\text{near}},j}, \hat{\mathcal{I}}_{i,j_{\text{near}}}) + \underbrace{\nabla_x \log p(\hat{\mathcal{I}}_{i_{\text{near}},j}, \hat{\mathcal{I}}_{i,j_{\text{near}}})}_{=0} \\ &= \nabla_x \log p(\hat{I}_{i,j} | \hat{\mathcal{I}}_{i_{\text{near}},j}, \hat{\mathcal{I}}_{i,j_{\text{near}}}) p(\hat{\mathcal{I}}_{i_{\text{near}},j}, \hat{\mathcal{I}}_{i,j_{\text{near}}}) \\ &= \nabla_x \log p(\hat{I}_{i,j}, \hat{\mathcal{I}}_{i_{\text{near}},j}, \hat{\mathcal{I}}_{i,j_{\text{near}}}). \end{aligned} \quad (16)$$

This suggests the score of  $I_{i,j}$  is only related to  $\hat{\mathcal{I}}_{i_{\text{near}},j}$  and  $\hat{\mathcal{I}}_{i,j_{\text{near}}}$ . Similar to the derivation in equation (9), we can achieve:

$$\nabla_x \log p(\hat{\mathcal{I}}) = \nabla_x \log \frac{p(\hat{I}_{i,j}, \hat{\mathcal{I}}_{i_{\text{near}},j}) p(\hat{I}_{i,j}, \hat{\mathcal{I}}_{i,j_{\text{near}}})}{p(\hat{I}_{i,j})}. \quad (17)$$

Finally, by further decomposing the numerator and applying the condition of continuity, we have:

$$\begin{aligned} \nabla_x \log p(\hat{\mathcal{I}}) &= \nabla_x \log \frac{p(\hat{\mathcal{I}}_{i,j} | \hat{\mathcal{I}}_{i_{\text{near}},j}) p(\hat{\mathcal{I}}_{i_{\text{near}},j}) p(\hat{\mathcal{I}}_{i,j} | \hat{\mathcal{I}}_{i,j_{\text{near}}}) p(\hat{\mathcal{I}}_{i,j_{\text{near}}})}{p(\hat{I}_{i,j})} \\ &\approx \nabla_x \log \frac{p(\hat{\mathcal{I}}_{i,j} | \hat{\mathcal{I}}_{-i,j}) p(\hat{\mathcal{I}}_{-i,j}) p(\hat{\mathcal{I}}_{i,j} | \hat{\mathcal{I}}_{i,-j}) p(\hat{\mathcal{I}}_{i,-j})}{p(\hat{I}_{i,j})} \\ &= \nabla_x \log \frac{p(\hat{\mathcal{I}}_{\{1:V\},j}) p(\hat{\mathcal{I}}_{i,\{1:F\}})}{p(\hat{I}_{i,j})} \\ &= \nabla_x \log p(\hat{\mathcal{I}}_{\{1:V\},j}) + \nabla_x \log p(\hat{\mathcal{I}}_{i,\{1:F\}}) - \nabla_x \log p(\hat{I}_{i,j}). \end{aligned} \quad (18)$$

Now we have verified the correctness of the conclusion in equation 9. Based on the similar derivation, we can also ensure the safety of equation (7). This guarantees the correctness of our main theorem.  $\square$

#### A.4 Additional implementation details

**Dataset and evaluate setting** In the main text, we test the proposed approach on three types of prompts: reference image, single-view video, and multi-view images of static 3D model. The



inputs used in our experiments for the first two tasks are respectively sourced from Animate124 [57] and Consistent4D [16], while that of the latter is collected from objaverse [8]. For the quantitative evaluation in the video-to-4D task, we follow Consistent4D’s testing protocol, reporting the average clip similarity across videos from four rendered views of all test examples. For the user study in the image-to-4D task, we collect the preferences of 50 participants on eight samples selected in Animate124 dataset, namely: astronaut-horse, cat-wave, eagle-fly, flag-wave, fox-game, lion-roar, monkey-bike, panda-dance.

**Condition generation** Since there is a slight domain gap between the training data of video diffusion models and the background removed view-fixed single object video in our task, the video generation model within our framework is often responsible for most of the failure cases and corrupted areas. Inspired by FreeInit [48], we let informative spatial-temporal low-frequency components of the initial latent guide the generation for these out-of-domain videos to create the ideal layout in the early denoising stage. Specifically, we repeated the sampling process twice, and set the initial noise for the second sampling process as follows:

$$x_T = \frac{x_0 + \sigma_T \mathbf{n}}{\sqrt{1 + \sigma_T^2}}, \quad (19)$$

where  $x_0$  is the primary denoised latent,  $\sigma_T$  is the initial noise level, and  $\mathbf{n} \sim \mathcal{N}(\mathbf{0}, \mathbf{I})$  is the same Gaussian noise used to generate  $x_0$  in the first sampling process. Experimental results indicate that this trick can effectively stabilize the generation, and the resulting significant reduction of failure cases cannot be achieved by trivially doubling the number of inference steps, which is aligned with the observations in [48]. To minimize the influence on efficiency, we used only 25 steps in the first sampling process.

**Image matrix generation** We also observed that the employed video diffusion model exhibits a noticeable view bias and struggles to stably generate side-view videos without clear semantics. Consequently, in the image matrix generation, we further adaptively tune the mixing weights for different views. Specifically, let  $s_i$  and  $r_i = 1 - s_i$  denote the weights of the video and multi-view score at the  $i$ -th sampling step in the logistic schedule. The weights adjusted by the view schedule are:

$$\begin{aligned} s'_i &= \alpha s_i \\ r'_i &= 1 - \alpha + \alpha r_i \\ \alpha &= \frac{1}{2} \times \left( 1 + \cos \frac{2\pi(x+1)}{10.5} \right) \end{aligned} \quad (20)$$

where  $v$  denotes the index of the view. This schedule reduces the contribution of the video generation model for the generation of side views.

## A.5 Additional results

**Text-to-4D generation** Naturally, *Diffusion*<sup>2</sup> is also capable of text-to-4D generation. Although the text-to-video-to-4D approach sounds more reasonable since it allows control of the dynamics using natural language, existing video generation models fail to achieve satisfactory performance in practice. Therefore, for the text-to-4D task, we finally opted for the more stable text-to-image-to-4D generation approach, *i.e.*, using image as the intermediary. Specifically, given a text prompt, we first synthesize the corresponding image. Subsequently, we perform background removal and recenter for the image to ensure the consistent use of the image extents with the training data of the multi-view diffusion model. Finally, the processed image is fed into our image-to-4D generation pipeline to synthesize the desired 4D assets. Actually, in Figure 3a, there are already some input images that are AI-generated. In Figure 6, we demonstrate more generated 4D assets from text prompts.

**4D reconstruction from partial views** To evaluate our method more comprehensively, we designed a quantitative benchmark, that assesses the fidelity of 4D reconstruction partial observation. Specifically, we render the front-view video and multi-view images at the reference frame from the animated 3D model as the condition for our generation pipeline. In Table 3, we report the PSNR and SSIM computed between generated frames and those rendered from six ground truth animated models collected from Maximo. For comparison, we evaluate the performance of Consistent4D

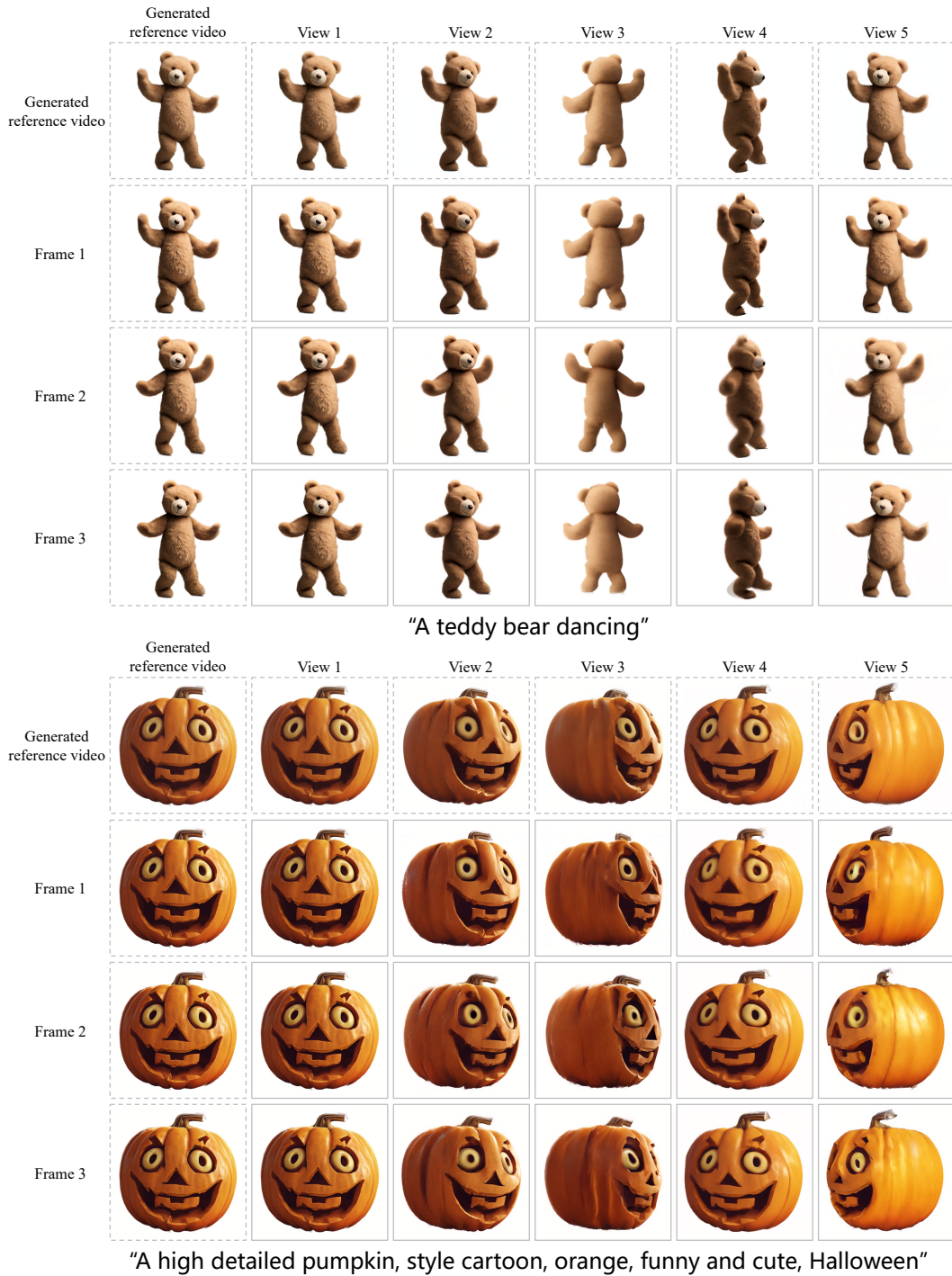


Figure 6: **Text-to-4D results.** We first generate an image conditioned on the text prompt and then perform our image-to-4D generation pipeline.

under this setting. To adapt it to this task, we render the same view and timestamp using the camera intrinsic of Zero-1-to-3 [22], and incorporate pixel-wise reconstruction loss of reference views in the Consistent4D pipeline. From the qualitative comparisons in Figure 7, it can be seen that the baseline methods are inferior in terms of detail fidelity and geometric consistency with reference view. Moreover, we also demonstrate an advantage in the quantitative metrics presented in Table 3, which can boil down to a better alignment with ground truth camera parameters, as the qualitative metrics are largely dominated by the layout of the synthesized views in this task. These results once again confirm our superiority over the baseline method.

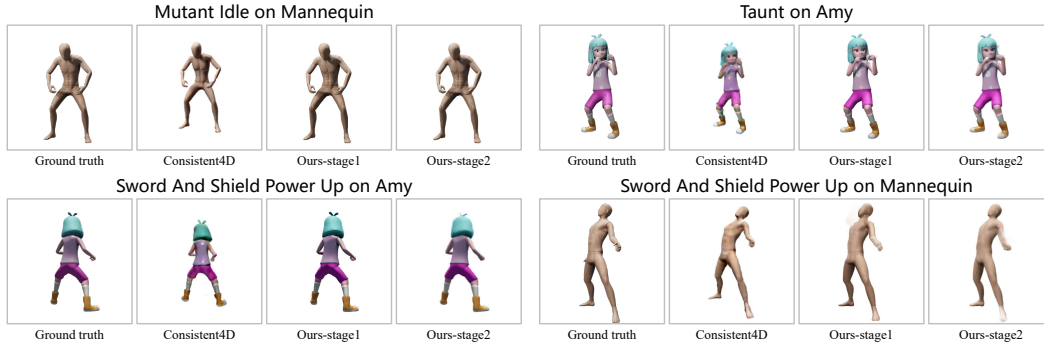


Figure 7: **Partial reconstruction results.** The synthesized images are conditioned on the reference single-view video and multi-view images.

Table 3: Quantitative comparison on the 4D reconstruction from partial observation.

Method	PSNR $\uparrow$	SSIM $\uparrow$
Consistent4D [16]	18.41	0.87
<i>Diffusion</i> <sup>2</sup> -stage1	20.45	0.89
<i>Diffusion</i> <sup>2</sup> -stage2	<b>21.55</b>	<b>0.90</b>